耦联剂辅助吸附法制备CuInS₂量子点敏化太阳电池

王　楠[1,2,#]　　梁柱荣[2,3,#]　　王　欣[1,2]　　徐雪青[2,3,*]　　方　军[1,*]　　王军霞[2,3]　　郭华芳[2,3]

([1]厦门大学化学与化工学院化工与生物工程系, 福建 厦门 361005; [2]中国科学院广州能源研究所,
中国科学院可再生能源与天然气水合物重点实验室, 广州 510640; [3]中国科学院大学, 北京 100049)

摘要： 分别以CuI和InAc₃作为铜源和铟源, 十二硫醇(DDT)作为硫源, 采用直接加热法合成不同尺寸的CuInS₂ (CIS)量子点. 运用X射线衍射(XRD), 拉曼光谱(Raman), 高分辨率透射电镜(HRTEM), 紫外-可见(UV-Vis)吸收光谱表征其相结构、形貌及光学性能. 结果表明: 制备的CIS量子点为黄铜矿结构, 且随着时间的延长, 量子点逐渐长大, 吸收光谱的激子吸收峰逐渐红移, 表现出量子尺寸效应. 采用巯基乙酸为双功能耦联剂辅助吸附法制备CIS敏化的TiO₂薄膜. 通过衰减全反射红外光谱(ATR-FTIR)分析得出, 巯基乙酸上的羧基与TiO₂表面羟基连接, 另一端上的巯基代替长链的DDT与CIS耦联, 将CIS成功锚定在TiO₂表面. 该方法不仅操作简单, 而且容易实现CIS在TiO₂表面的吸附. 太阳电池光电性能测试表明, 粒径大小约为3.6 nm的CIS量子点表现出最优的吸附能力以及光电转换性能. 进一步采用连续离子吸附层法对CIS敏化的TiO₂薄膜进行CdS包覆, 光电转换性能大大提高, 其效率达到2.83%, 这主要源于CdS的包覆钝化了CIS的表面缺陷, 有效地降低了电子复合.

关键词： 铜铟硫; 量子点; 敏化太阳电池; 多功能耦联剂; 巯基乙酸; 辅助吸附

中图分类号： O649

CuInS₂ Quantum Dot-Sensitized Solar Cells Fabricated *via* a Linker-Assisted Adsorption Approach

WANG Nan[1,2,#]　　LIANG Zhu-Rong[2,3,#]　　WANG Xin[1,2]　　XU Xue-Qing[2,3,*]

FANG Jun[1,*]　　WANG Jun-Xia[2,3]　　GUO Hua-Fang[2,3]

([1]Department of Chemical & Biochemical Engineering, College of Chemistry and Chemical Engineering, Xiamen University, Xiamen 361005, Fujian Province, P. R. China; [2]Renewable Energy and Gas Hydrate Key Laboratory of Chinese Academy of Sciences, Guangzhou Institute of Energy Conversion, Chinese Academy of Sciences, Guangzhou 510640, P. R. China; [3]University of Chinese Academy of Sciences, Beijing 100049, P. R. China)

Abstract: Colloidal chalcopyrite CuInS₂ (CIS) quantum dots (QDs) were synthesized using copper(I) iodine (CuI) and indium(III) acetate (InAc₃) as metal cationic precursors, and dodecanethiol (DDT) as the sulfur source and solvent. The microstructure and optical properties of the prepared CIS QDs were characterized by X-ray diffraction (XRD), Raman spectroscopy, high-resolution transmission electron microscopy (HRTEM), and UV-Vis absorption spectroscopy. The results showed that the CIS consisted of chalcopyrite phase and exhibited Cu-Au ordering. With prolonged reaction time, the grain sizes of the QDs became larger and the absorption edges of the CIS QDs showed a red-shift owing to the size-induced quantum confinement effect. For the first

time, DDT-capped CIS QDs with narrow size distribution were connected to the inner surface of mesoporous TiO_2 films *via* a thioglycolic acid (TGA)-assisted adsorption approach, which was simple and easy to carry out. The adsorption behaviors of both TGA and the CIS QDs on the TiO_2 films were detected by attenuated total reflectance Fourier transform infrared (ATR-FTIR) spectroscopy. The results indicated that TGA was adsorbed onto the surface of TiO_2 *via* COOH groups while the −SH group was exposed outside, and replaced DDT at the surface of the CIS QDs, leading to the attachment between TiO_2 and CIS. It was revealed that the CIS QDs of ~3.6 nm in size exhibited the best light absorption capacity and photovoltaic performance. An over-coating of CdS significantly improved the performance of the QDSSCs owing to decreased electron recombination, and a power conversion efficiency of ~2.83% was obtained.

Key Words: $CuInS_2$;   Quantum dot;   Sensitized solar cell;   Bifunctional linker;   Thioglycolic acid;   Assisted adsorption

1 Introduction

Quantum dot-sensitized solar cells (QDSSCs) have attracted great attention as a promising alternative to conventional microporous dye-sensitized solar cells due to their low cost, tunable band gap,[1] high absorption coefficient,[2] and multiple excition generation.[3] In particular, ternary copper indium sulphide ($CuInS_2$, CIS in brief) quantum dots (QDs) have been considered as an emerging candidate to the most widely used heavy metal-based binary QDs (e.g., CdSe and CdTe) for its optimal direct bulk band gap (ca 1.5 eV),[4] low-toxicity, and appreciable electrochemical stability.

For the fabrication of QDSSCs, QDs can be deposited onto the mesoporous wide-bandgap semiconductors (WDSCs), such as TiO_2, ZnO, or SnO_2 by two classes of methods: *in situ* and *ex situ*. *In situ* methods include chemical bath deposition (CBD),[5] successive ionic layer adsorption and reaction (SILAR),[6] electrophoresis deposition,[7] and thermal decomposition,[8] etc., which ensure the high surface coverage of QDs.[9,10] However, the lack of capping ligands usually results in a broad QDs size-distribution, and a huge amount of surface trap states, which arouse potentially detrimental recombination. Alternatively, *ex situ* deposition approach is competent in terms of the homogenous QD size and crystal structure, which needs to prepare the colloidal QDs prior to incorporating them onto the TiO_2 electrodes. To assemble the colloidal QDs onto the WDSCs, bifunctional linkers of HS-R-COOH, such as mercaptopropionic acid (MPA), thiolacetic acid (TAA), mercaptohexadecanoic acid (MDA), and thioglycolic acid (TGA) have been adopted. For instance, Li *et al.*[11] have prepared MPA-capped CIS QDs from hydrophobic oleyamine-capped CIS QDs *via* ligand exchange approaches to deposit CIS QDs onto the mesoporous TiO_2 films, and a remarkable power conversion efficiency (PCE) of 4.2% has been achieved combined with surface coating of CdS *via* SILAR. Meng *et al.*[12] employed a self-assembly method to assemble the hydrophilic MPA-capped CIS QDs onto the TiO_2 films, followed by growing a CdS shell on the surface, which enhanced the PCE to ~4.69%. Chang *et al.*[13] reported a so-called two-step ligand exchange method to prepare MPA coated CIS QDs, and a maximum PCE of 1.84% has been achieved by further combining *in situ* growth approaches for Cd-free CIS QDSSCs.

It is worth noting that the ligand exchange approaches are complicated and need special technics. It is of great interest to look for facile alternative method to attach the CIS QDs to TiO_2 films. In this paper, CIS QDs were linked with TiO_2 films *via* bifunctional linker-assisted adsorption approach which has been widely investigated for TOP-capped CdSe QDs.[14] For the first time, the DDT-capped CIS QDs were connected onto TiO_2 films with TGA-assisted, resulting in a high surface coverage and strong electronic coupling between QDs and TiO_2. With an over coating of CdS *via* SILAR, a relatively high PCE of ~2.8% has been obtained.

2 Experimental

2.1 Materials

Copper(I) iodine (CuI, 99.99%), dodecanethiol (DDT, 99%), indium(III) acetate ($InAc_3$, 99.90%) and thioglycolic acid (TGA, >90%) were purchased from Aladdin Chemistry Co., Ltd. $Na_2S \cdot 9H_2O$ (98%), $Cd(NO_3)_3 \cdot 4H_2O$ (99%), $Zn(OAc)_2 \cdot 2H_2O$ (99%), NaOH (99%), S (99%), and hexane (99.9%) were obtained from Guangzhou Chemical Reagent Co., Ltd. TiO_2 pastes: (TPP3, average size 20 nm) from HeptaChroma Co., Ltd. were used to prepare TiO_2 nanoparticles for photoelectrodes. Titanium(IV) chloride tetrahydrofuran complex ($TiCl_4 \cdot 2THF$, 97%) was from Sigma-Aldrich. All the chemicals were used without further purification.

2.2 Preparation of CIS QDs

The CIS QDs were synthesized *via* a heating-up method based on previously reported methods.[15] Copper(I) iodine (CuI) (0.07935 mg, 0.416 mmol) and indium(III) acetate ($InAc_3$) (0.146 mg, 0.5 mmol) were dissolved in dodecanethiol (DDT) in a 50 mL three-necked flask with vigorous magnetic stirring, where DDT acts as both a sulfur source and solvent. The reaction mixture was degassed under vacuum for 5 min and purged with nitrogen for 5 min, subsequently raised to 100 °C, and maintained for 10 min until a clear mixture was formed. Finally the temperature was heated to 230 °C and kept for different reaction time, i.e., 5, 10, 15, and 20 min. The reaction mixture was precipitated by the addition of ethanol and dispersed in hexane for storage. The obtained samples at different time were named as CIS-5 min, CIS-10 min, CIS-15 min, and CIS-20 min, respectively.

2.3 Preparation of CIS and CIS/CdS sensitized TiO₂ films

A ~100 nm compact TiO₂ layer was deposited on the FTO by spray pyrolysis of 0.2 mol·L⁻¹ titanium(IV) bis(acetoacetonato)di(isopropanoxylate) to retard the electron recombination at FTO/electrolyte interface.[16] A microporous transparent TiO₂ film composed of 20 nm particles was doctor bladed on top of the blocking layer. Afterwards, a dispersion of scattering TiO₂ particles was screen-printed on top of the transparent film; the electrodes were annealed at 450 °C for 30 min, followed by dipping in an aqueous solution of titanium(IV) chloride tetrahydrofuran complex (TiCl₄·2THF) (30 mmol·L⁻¹) at 70 °C before sintering at 500 °C for 30 min. For sensitization, the TiO₂ films were pre-treated by soaking in 15 mL of ethanol containing 30 mmol·L⁻¹ TGA for 12 h. After rinsed with ethanol, the TGA-modified TiO₂ films were directly immersed into CIS QDs (10 mmol·L⁻¹)/hexane solution for 24 h at room temperature. For the ex situ growth of CdS layers, the TiO₂/CIS QD electrodes were successively immersed in two different solutions for 60 s each: (1) 0.05 mol·L⁻¹ Cd(NO₃)₂·4H₂O in methanol, and (2) 0.05 mol·L⁻¹ Na₂S·9H₂O in methanol. Following each immersion, the electrodes were rinsed with methanol to remove the excess of each precursor solution. The SILAR process was repeated for 6 cycles. And the CIS QDs, CdS, and CIS/CdS sensitized TiO₂ films are named as TiO₂/CIS, TiO₂/CdS, TiO₂/CIS/CdS, respectively. All the electrodes fabricated here have been coated with ZnS via two SILAR cycles by subsequently dipping in 0.1 mol·L⁻¹ Zn(NO₃)₂·2H₂O and 0.1 mol·L⁻¹ Na₂S·9H₂O aqueous solutions for 60 s each time.

2.4 Fabrication of CIS and CIS/CdS QDSSCs

The CIS QDSSCs were prepared by assembling a QDs-sensitized electrode and Cu₂S counter electrode using a polysulfide electrolyte. The polysulfide redox electrolyte consisted of 1 mol·L⁻¹ Na₂S·9H₂O, 1 mol·L⁻¹ S, and 0.1 mol·L⁻¹ NaOH solutions in 10 mL ultrapure water. The Cu₂S counter-electrodes were prepared by immersing brass in hydrochloric acid at 70 °C for 45 min, followed by dropping polysulfide electrolyte onto the brass for 1 min, resulting in porous Cu₂S electrodes.

2.5 Characterization

X-ray diffraction (XRD) patterns were obtained on an X' pert pro MPD X-ray diffract meter using Cu K_a irradiation at a scan rate (2θ) of 0.0167 (°)·s⁻¹. The accelerating voltage and applied current were 40 kV and 80 mA, respectively. High-resolution transmission electron microscope (HRTEM) images were obtained with a Philips CM200 FEG TEM operated at 200 kV. Scanning electron microscopic (SEM) images were obtained using an S-4800 High resolution field emission SEM (FESEM, Hitachi, Japan). Energy dispersive X-ray (EDX) spectra were performed on a Hitachi S-4800 field emission scanning electron microscope with an Oxford instruments Inca EDX system operated at 20 kV. Raman spectra of the CIS were detected on a Lab RAM HR800 with the excitation wavelength of 532 nm. The diffuse reflection and transmission spectra of the QDs-sensitized TiO₂ electrodes

have been carried out with a Shimadzu UV-2401 UV-Vis spectrophotometer, and the absorption spectra of the samples were obtained according to absorption (%)=100% −transmittance (T)−reflectance (R). The attenuated total reflectance flourier transform infrared (ATR-FTIR) spectra of the TiO₂ films were obtained using a Nicolet 210 FTIR spectrophotometer. The photocurrent density−potential (J−V) characteristics of the devices were measured with a FRA-equipped type III electrochemical work station from Auto Lab. The cells were illuminated using the ABET Sun 3000 solar simulator at AM 1.5G, where the light intensity was adjusted with an NREL-calibrated silicon solar cell to one sun illumination (100 mW·cm⁻²).

3 Results and discussion

3.1 Phase structure, composition and optical properties of the CIS QDs

Colloidal chalcopyrite CIS QDs have been synthesized with CuI and InAc₃ as metal cationic precursors, DDT as sulfur source and solvent with Cu/In molar ratio of 1/1.2. Fig.1(a) presents the UV-Vis absorption spectra of the CIS QDs synthesized at 230 °C for different reaction time. The absorption edges showed an obvious red-shift when the reaction time was prolonged from 5 min to 20 min. As CIS is a direct transition semiconductor, the photon energy was calculated by a least-squares fit of the linear region of $(Ah\nu)^2$ vs $h\nu$ plot in the top right corner of Fig.1(a), where A is absorbance, and h is the Planck constant. It can be seen that the optical band gaps of the CIS QDs varied from 1.82, 1.76, 1.73 eV to 1.69 eV with the reaction time prolonged from 5, 10, and 15 min to 20 min, owing to the growth of the CIS QDs which exhibited quantum confinement effect. The TEM images and size distribution diagram of CIS QDs obtained at 230 °C for 15 min are presented in Fig.1(b). It can be seen that the CIS QDs were uniform and in the triangular-like shape with an average diameter of 3.6 nm, slightly smaller than the Bohr diameter of CIS (around 8.1 nm).[17]

Fig.1(c) exhibits the XRD pattern of the CIS QDs synthesized at 230 °C for 15 min, which could be assigned to the chalcopyrite CIS (JCPDS 85-1575).[18−20] Average grain size calculated from the half peak width of the (112) lattice plane employing the Debye-Scherer formula was about ~5 nm, which was larger than the result from HRTEM observations. The two co-existence phases were expected in CIS materials, one is chalcopyrite ordered phase and the other is Cu-Au ordered phase. The latter is derived from the chalcopyrite ordered phase and related with the anti-site defect states. To obtain more accurate information on the phase composition of the prepared samples, Raman spectrum of the as-synthesized CIS QDs was further detected as shown in Fig.1(d). The intensive bands at 259, 294, and 340 cm⁻¹ belong to the E_3, A_1, and B_{23} modes of the chalcopyrite structure, respectively. It is worth remarking that an additional band at 305 cm⁻¹ was also detected,[21] which can be assigned to the A_1^* band of Cu-Au ordering, resulting in undesirable deep defect states.
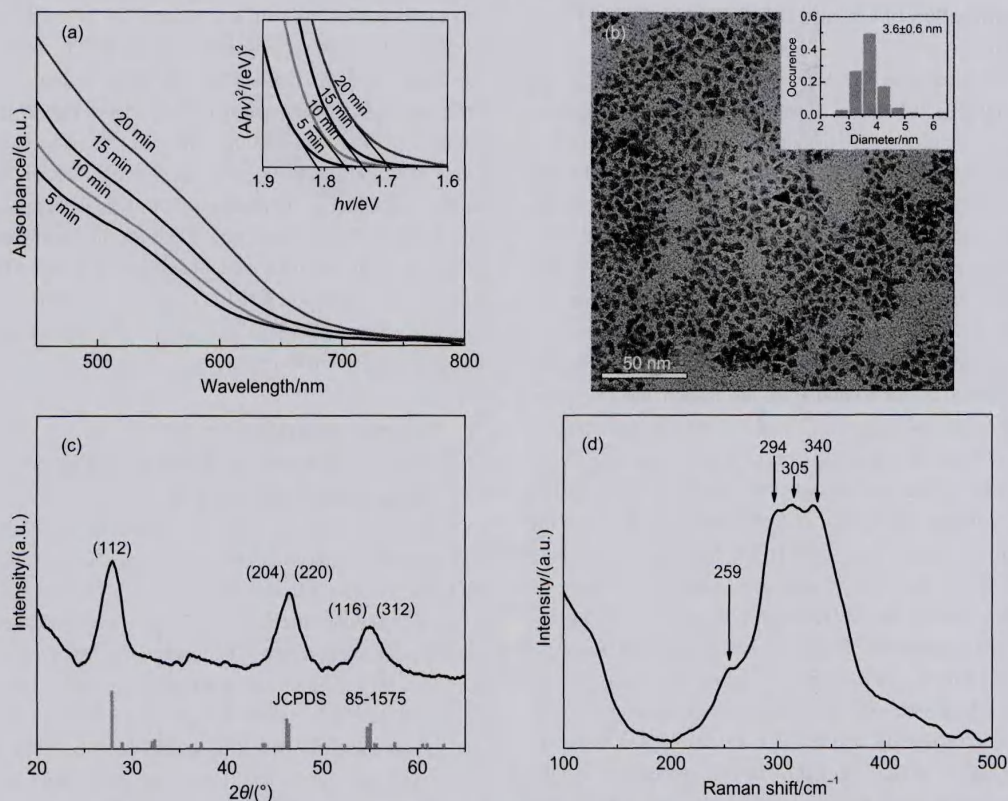
3.2 CIS and CIS/CdS sensitized TiO₂ films

Fig.1 (a) Absorption spectra of CIS QDs synthesized at 230 °C for different reaction time, and inset in the right corner is the plots of $(Ahv)^2$ as a function of energy (hv); (b) TEM image and size distribution diagram; (c) XRD patterns and (d) Raman spectra of the CuInS$_2$ QDs synthesized at 230 °C for 15 min

To attach CIS QDs to TiO$_2$ surface, a bifunctional linker-assisted adsorption approach has been adopted. The procedure for fabrication process of the CuInS$_2$ QDs sensitized TiO$_2$ photo anode is illustrated schematically in Fig.2(a). Firstly, the TiO$_2$ films were dipped into the TGA solution. Then, the TGA-modified TiO$_2$ films, named as TiO$_2$/TGA, were further immersed into the DDT-capped CIS QDs solutions. The TiO$_2$ films became brown after about 24 h, indicating that they have been coated with CIS QDs. To realize the interactions between TGA and the DDT-capped CIS, the ATR-FTIR spectra of the TiO$_2$, TiO$_2$/CIS, TiO$_2$/TGA films,

and CIS QDs were measured and presented in Fig.2(b), and the vibration band assignments of the spectra are listed in Table 1. In the case of DDT-capped CIS, two obvious bands at 2935 and 2847 cm^{-1} are corresponded to stretching vibration of $-$CH$_3$ groups in DDT. For TiO$_2$/TGA, the band at 1550 and 1460 cm^{-1} can be attributed to the COO-Ti groups, and the bands at 2556 and 721 cm^{-1} were assigned to $-$SH and C$-$S stretching vibration, respectively. It can be imagined that the TGA is sufficiently anchored onto the surface of TiO$_2$ through the carboxyl group $-$COOH and with the mercapto group $-$SH exposed outside. By

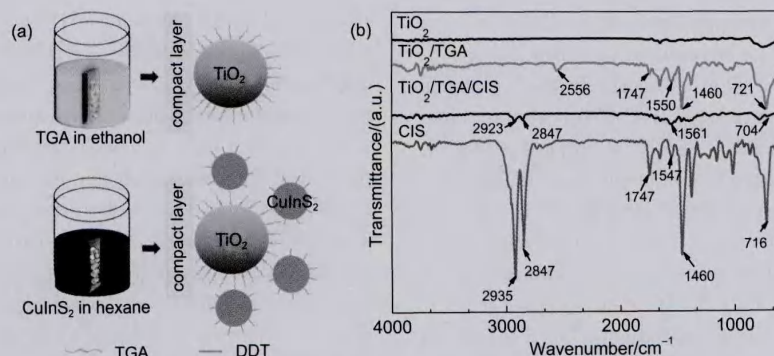**Fig.2** (a) Schematic illustration of the fabrication process of the CuInS$_2$ QDs sensitized TiO$_2$ photo anode; (b) ATR-FTIR spectra of the TiO$_2$, TiO$_2$/TGA, TiO$_2$/CIS films, and the free CIS QDs

**Table 1　Vibration band assignments of the ATR-FTIR spectra for the CIS QDs, TiO$_2$/TGA, and TiO$_2$/CIS films**

Vibrational mode [a]		v/cm^{-1}		
		CIS	TiO$_2$/TGA	TiO$_2$/CIS
—CH$_3$	v_{as}, CH$_3$	2935	–	2923
	v_s, CH$_3$	2847	–	2847
—SH	v, S—H	–	2556	–
—H$_2$C—S	v, C—S	716	721	704
—COOM	v_s, O=C=O	1547	1550	1561
	v_{as}, O=C=O	1460	1460	1459
—COOH	v, C=O	1747, 1651	1747, 1652	1744, 1652
	v, O—H	3747	3747	3747

further sensitized with DDT-capped CIS, the absorption bands belonging to —SH disappeared, and at the meantime the bands belonging to —CH$_3$ for CIS QDs weakened, which indicated that CIS has been linked with TiO$_2$ *via* —SH group and released the long-chain ligand DDT into the solution. In addition, 1747, 1651, and 1547 cm^{-1} for CIS might be related to the COO-In groups which suggested that —COO$^-$ group released from InAC$_3$ have coordinated with CIS.

For the purpose of detecting the light-harvesting property of QDs-sensitized TiO$_2$ electrodes for different reaction time, the diffuse absorption of the samples have been obtained according to the following equation: absorption (%)=100%−T−R. As shown in Fig.3(a), the absorption edges of the CIS sensitized TiO$_2$ electrodes underwent a progressive red-shift with the reaction time prolonged, corresponding to the color change of the photo anodes in the top right corner, which was in good agreement with the results shown in Fig.1(a). However, the absorption intensities of the electrodes sensitized with CIS-20 min are slightly lower
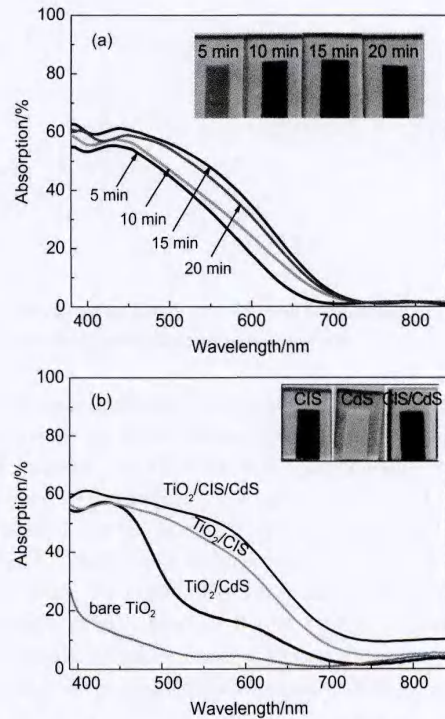
Fig.3　UV-Vis absorption spectra of (a) the TiO$_2$ film sensitized with CIS QDs grown at 230 °C for 5, 10, 15, 20 min and (b) the films of the bare TiO$_2$, TiO$_2$/CIS, TiO$_2$/CdS, and TiO$_2$/CIS/CdS

than that of the CIS-15 min. This can be ascribed mainly to the larger grain size of the CIS-20 min, which was unfavorable to be attached onto the inner surface of TiO$_2$ films. For this reason, the CIS-15 min was mainly investigated.
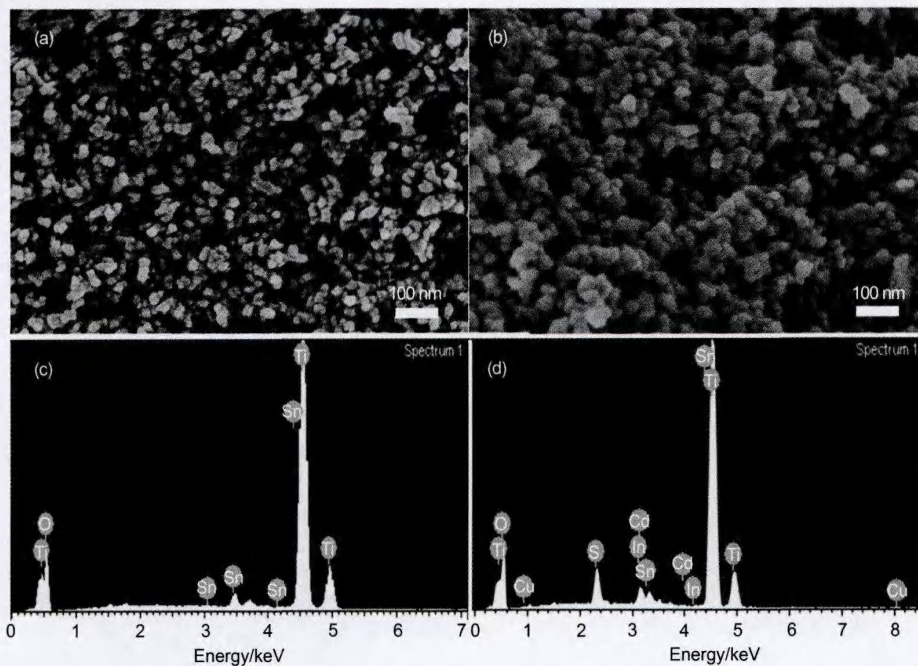
Fig.4　SEM images for the top-view of the TiO$_2$ films (a) before sensitization and (b) coated with the CIS/CdS; EDX spectra for the TiO$_2$ films (c) before sensitization and (d) coated with the CIS/CdS
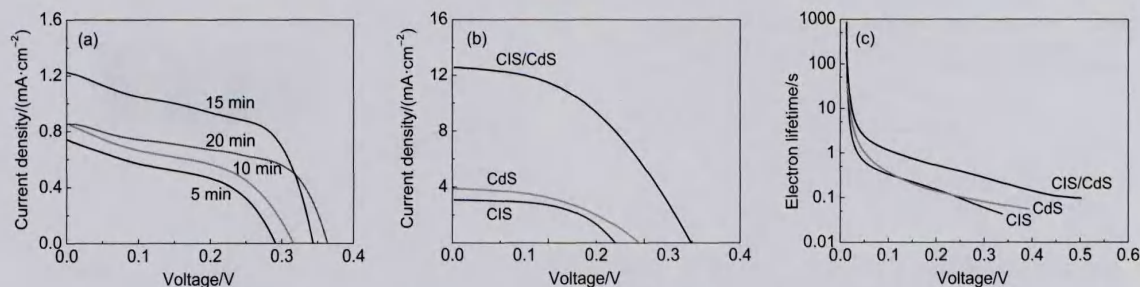
Fig.5 (a) Photocurrent density–voltage characteristic curves for different time of CIS; (b) current density–voltage characteristic curves, and (c) electron lifetimes of the solar cells based on TiO₂/CdS, TiO₂/CIS, and TiO₂/CIS/CdS electrodes

In order to further inhibit electron recombination, CdS was coated onto the CIS-15 min sensitized TiO₂ films. Fig.3(b) presents the UV-Vis absorption of the bare TiO₂ film, TiO₂/CdS, TiO₂/CIS, and TiO₂/CIS/CdS films, which showed that the absorption onsets of the films were 560, 720, and 750 nm, respectively. Notably, the light absorption intensities of the TiO₂/CIS/CdS were greatly enhanced ranging from 400 to 800 nm.[22] Shown in the right corner of Fig.3(b), the TiO₂/CIS and TiO₂/CdS films were originally reddish-brown and pale yellow, respectively. When the TiO₂/CIS was further coated with CdS, the films became dark-brown.

Fig.4(a, b) shows the SEM images of the bare TiO₂ films and those coated with CIS/CdS. The bare TiO₂ film was a uniform network of TiO₂ nanoparticles with average sizes of around 20 nm. After being treated with CIS QDs and CdS, the size of the nanoparticles became larger (approximately 27 nm), the pores between the TiO₂ nanoparticles become smaller but still remain open, which favors the effective penetration of electrolyte and is beneficial to the photo generated holes transport in QDSSCs.[23–25] Furthermore, as shown in Fig.4(d), the Cd, Cu, and In elements can be found in EDX spectra of the CIS/CdS sensitized TiO₂ film, which further reveals that the CIS and CdS have been successfully adsorbed onto the surface of TiO₂ nanoparticles.

3.3 Photo electrochemical performance of the devices

The photocurrent density–voltage (J–V) curves of the solar cells based on CIS QDs obtained from different times were measured under standard AM 1.5G illumination (100 mW·cm⁻²) and presented in Fig.5(a). The corresponding photovoltaic parameters of cells are summarized in Table 2. The results indicated that the TiO₂/CIS-15 min sample exhibited the best photo-

voltaic performance with a highest short-circuit current density (J_{sc}), fill factor (FF), and PCE, which was beneficial from the light-harvesting enhancement as shown in Fig.3(a), and also originated from its lower defect states.

Accordingly, CIS QDSSCs based on CIS-15 min QDs have been further optimized and treated with CdS. Fig.5(b) presents the photocurrent density–voltage curves of solar cells based on TiO₂/CdS, TiO₂/CIS and TiO₂/CIS/CdS electrodes. Compared with the TiO₂/CdS and TiO₂/CIS QDSSCs, the hybrid-sensitized TiO₂/CIS/CdS solar cells exhibited a PCE of 2.83%, which was almost 5 times higher than pristine CdS solar cells. The CdS layers can significantly passivate the CIS QDs surface defects and apparently inhibit the charge recombination at the TiO₂/CIS interface, resulting in much higher J_{sc}, V_{oc}, FF, and hence PCE.

In order to gain more information on the electron recombination behavior of the solar cells, the electron lifetimes have been

Table 2 Detail photovoltaic parameters of QDSSCs

Photo anode	V_{oc}/V	J_{sc}/(mA·cm⁻²)	FF/%	PCE/%
CIS-5 min	0.29	0.74	0.46	0.10
CIS-10 min	0.32	0.85	0.50	0.14
CIS-15 min	0.34	1.20	0.53	0.22
CIS-20 min	0.36	0.85	0.52	0.16
CdS	0.38	3.87	0.45	0.66
CIS	0.34	2.80	0.55	0.51
CIS/CdS	0.50	12.6	0.45	2.83

V_{oc}: open-circuit voltage; J_{sc}: short-circuit current density; FF: fill factor
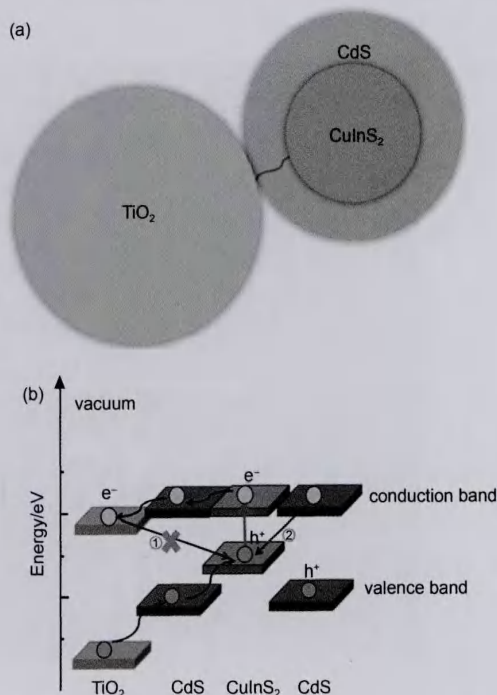
Fig.6 (a) Schematic illustration and (b) energy band diagram of the CIS/CdS QDs sensitized TiO₂

derived from open circuit voltage decay measurement and shown in Fig.5(c). Longer electron lifetime achieved in TiO₂/CIS/CdS solar cells refers to a relatively lower recombination rate, indicating that the undesirable charge leakage at the interface has been suppressed by the hybrid-sensitized structure, which is in good agreement with the results from $J-V$ measurements. It is worth noting that the electron lifetime is much higher than the QDSSCs based on SILAR approach in our previous studies.[16] As shown in Fig.6(a), a core-shell model is formed, and the energy band diagram is displayed in Fig.6(b). The recombination in the CIS-sensitized solar cell is dominated by electron transfer from the conduction band of TiO₂ to the unoccupied defeat states and valence band in CIS, as indicated in our previous work. The CdS layer decreases the probability of electron recombination at TiO₂/CIS interfaces (the route of ① in Fig.6(b)).[12] Furthermore, the unique feature makes the holes localized in CIS recombine with the electrons in conduction band of CdS (the route of ② in Fig.6(b)) efficiently, which led to efficient hole extractions. Nevertheless, exact understanding of electron injection and charge recombination kinetics in this system is still unambiguous and requires further systematic studies.

4　Conclusions

In conclusion, a simple bifunctional linker-assisted adsorption approach has been developed for the fabrication of the colloidal CIS QDs sensitized solar cells. For the first time, the DDT-capped CIS was linked with TiO₂ films *via* TGA. In addition, CIS QDs sensitized solar cells coated with CdS exhibited retarded electron recombination and efficient hole extraction, which led to an enhanced PCE of ~2.83% (J_{sc}=12.6 mA·cm⁻², V_{oc}=0.5 V, FF=0.45) under one-sun illumination. In the future, the photovoltaic perform of the solar cells is believed to be further improved by the optimization of the thickness of CdS, the grain size of CIS, and passivation with ZnS.[26]

References

(1)　Tian, J. J.; Cao, G. Z. *Nano Rev.* **2013**, *4*, 22578.

(2)　Hosseinpour-Mashkani, S. M.; Salavati-Niasari, M.; Mohandes, F. *Ind. Eng Chem.* **2014**, *20*, 3800. doi: 10.1016/j. jiec.2013.12.082

(3)　Beard, M. C. *J. Phys. Chem. Lett.* **2011**, *2*, 1282. doi: 10.1021/jz200166y

(4)　Booth, M.; Brown, A. P.; Evans, S. D.; Critchley, K. *Chem. Mater.* **2012**, *24*, 2064. doi: 10.1021/cm300227b

(5)　Pathan, H. M.; Lokhande, C. D. *Appl. Surf. Sci.* **2004**, *4*, 003.

(6)　Senthamilselvi, V.; Saravanakumar, K.; Jabena-Begum, N.; Anandhi, R.; Ravichandran, A. T.; Sakthivel, B.; Ravichandran, K. *J. Mater. Sci: Mater-Electron.* **2011**, *23*, 302.

(7)　Santra, P. K.; Nair, P. V.; Thomas, K. G.; Kamat, P. V. *J. Phys. Chem. Lett.* **2013**, *4*, 722. doi: 10.1021/jz400181m

(8)　Lutz, T.; MacLachlan, A.; Sudlow, A.; Nelson, J.; Hill, M. S.; Molloy, K. C.; Haque, S. A. *Phys. Chem. Chem. Phys.* **2012**, *14*, 16192. doi: 10.1039/c2cp43534a

(9)　Wang, Y. Q.; Rui, Y. C.; Zhang, Q. H.; Li, Y. G.; Wang, H. Z. *ACS Appl. Mater. Inter.* **2013**, *5*, 11858. doi: 10.1021/am403555c

(10)　Chen, Z. G.; Tang, M. H.; Song, L. L.; Tang, G. Q.; Zhang, B. J.; Zhang, L. S.; Yang, J. M.; Hu, J. Q. *Nanoscale Res. Lett.* **2013**, *8*, 354. doi: 10.1186/1556-276X-8-354

(11)　Li, T. L.; Lee, Y. L.; Teng, H. *Energy Environ. Sci.* **2012**, *5*, 5315. doi: 10.1039/C1EE02253A

(12)　Luo, J. H.; Wei, H. Y.; Huang, Q. L.; Hu, X.; Zhao H. F.; Yu, R. C.; Li, D. M.; Luo, Y. H.; Meng, Q. B. *Chem. Commun.* **2013**, *49*, 3881. doi: 10.1039/c3cc40715b

(13)　Chang, C. C.; Chen, J. K.; Chen, C. P.; Yang, C. H.; Chang, J. Y. *ACS Appl. Mater. Inter.* **2013**, *5*, 11296. doi: 10.1021/am403531q

(14)　Xu, X. Q.; Giménez, S.; Mora-Seró, I.; Abate, A.; Bisquert, J.; Xu, G. *Mater. Chem. Phys.* **2010**, *124*, 709. doi: 10.1016/j. matchemphys.2010.07.041

(15)　Li, L.; Pandey, A.; Werder, D. J.; Khanal, B. P.; Pietryga, J. M.; Klimov, V. I. *J. Am. Chem. Soc.* **2011**, *133*, 1176. doi: 10.1021/ja108261h

(16)　Xu, X. Q.; Wan, Q. C.; Luan, C. Y.; Mei, F. Q.; Zhao, Q.; An, P.; Liang, Z. L.; Xu, G.; Zapien, J. A. *ACS Appl. Mater. Inter.* **2013**, *5*, 10605. doi: 10.1021/am402502a

(17)　Torimoto, T.; Tada, M.; Dai, M. L.; Kameyama, T.; Suzuki, S.; Kuwabata, S. *J. Phys. Chem. C* **2012**, *116*, 21895. doi: 10.1021/jp307305q

(18)　Yin, Z.; Hu, Z. L.; Ye, H. H.; Teng, F.; Yang, C. H.; Tang, A. W. *Appl. Surf. Sci.* **2014**, *307*, 489. doi: 10.1016/j. apsusc.2014.04.063

(19)　Kolny-Olesiak, J.; Weller, H. *ACS Appl. Mater. Inter.* **2013**, *5*, 12221. doi: 10.1021/am404084d

(20)　Liu, Z. P.; Wang, L. L.; Hao, Q. Y.; Wang, D.; Tang, K. B.; Zuo, M.; Yang, Q. *CrystEngComm* **2013**, *15*, 7192. doi: 10.1039/c3ce40631h

(21)　Oja, I.; Nanu, M.; Katerski, A.; Krunks, M.; Mere, A.; Raudoja, J.; Goossens, A. *Thin Solid Films* **2005**, *80*, 480.

(22)　Li, T. L.; Lee, Y. L.; Teng, H. *J. Mater. Chem.* **2011**, *21*, 5089. doi: 10.1039/c0jm04276e

(23)　Li, J. Z.; Kong, F. T.; Wu, G. H.; Huang, Y.; Chen, W. C.; Dai, S. Y. *Acta Phys. -Chim. Sin.* **2013**, *29*, 1851. [李景哲, 孔凡太, 武国华, 黄　阳, 陈汪超, 戴　松. 物理化学学报, **2013**, *29*, 1851.] doi: 10.3866/PKU.WHXB201306172

(24)　Li, W. X.; Hu, L. H.; Dai, S. Y. *Acta Phys. -Chim. Sin.* **2011**, *27*, 2367. [李文欣, 胡林华, 戴松元. 物理化学学报, **2011**, *27*, 2367.] doi: 10.3866/PKU.WHXB20111011

(25)　Bisquert, J. *J. Phys. Chem. B* **2002**, *106*, 325. doi: 10.1021/jp011941g

(26)　Guo, X. D.; Ma, B. B.; Wang, L. D.; Gao, R.; Dong, H. P.; Qiu, Y. *Acta Phys. -Chim. Sin.* **2013**, *29*, 1240. [郭旭东, 马蓓蓓, 王立铎, 高　瑞, 董豪鹏, 邱　勇. 物理化学学报, **2013**, *29*, 1240.] doi: 10.3866/PKU.WHXB201303261